Journal of Photochemistry and Photobiology A: Chemistry 220 (2011) 94–101

Contents lists available at ScienceDirect

Journal of Photochemistry and Photobiology A: Chemistry

journal homepage: www.elsevier.com/locate/jphotochem

Effect of microwave radiation on the (Raman) lattice phonons in selected titanium dioxide solid specimens

Satoshi Horikoshi [a,b,*], Masahiko Abe [b], Susumu Sato [c], Nick Serpone [d,**]

[a] Department of Material & Life Science, Faculty of Science and Technology, Sophia University, 7-1 Kioicho, Chiyodaku, Tokyo 102-8554, Japan
[b] Research Institute for Science and Technology, Tokyo University of Science, 2641 Yamazaki, Noda, Chiba 278-8510, Japan
[c] Sensor Photonics Research Center, Toyo University, 2100 Kujirai, Kawagoe, Saitama 350-8585, Japan
[d] Gruppo Fotochimico, Dipartimento di Chimica, Universita di Pavia, Via Taramelli 10, Pavia 27100, Italy

ARTICLE INFO

Article history:
Received 20 December 2010
Received in revised form 28 March 2011
Accepted 31 March 2011
Available online 8 April 2011

Keywords:
TiO_2
Microwaves
Lattice vibrations
In situ Raman spectroscopy
Lattice phonons
Microwave-induced phenol photodegradation

ABSTRACT

The effects of 2.45-GHz microwave radiation on the Raman-active lattice phonons of two selected (Wako) anatase and rutile specimens and on Degussa P-25 TiO_2 nanoparticles were probed by *in situ* microscopic Raman spectroscopy in the solid phase with samples subjected to microwave irradiation (MW) or in combination with UV illumination (UV/MW). Significant changes were seen in the Raman band intensities for the pure anatase E_g mode at 143 cm^{-1} and for the rutile vibration at 446 cm^{-1}, whereas only negligible changes in intensity were observed for the 144 cm^{-1} band of P-25 nanoparticles exposed to MW and UV/MW radiation. It is deduced that microwaves have a negligible impact on the lattice vibrational modes (phonons) of P-25 titania, even though this specimen was thermally heated by the microwaves. The photodegradation of phenol was re-visited to examine the photoactivity of the TiO_2 specimens selected for the *in situ* Raman study, as attested by the number of $^{\bullet}OH$ radicals produced (DMPO spin trap ESR) under UV versus UV/MW irradiations, and by the related enhanced dynamics under UV/MW irradiation relative to UV alone or UV/CH.

1. Introduction

Literature of the past two decades has demonstrated convincingly the advantages of microwaves in syntheses, as the reaction times are shortened considerably from days to several minutes, often with significantly improved product yields. A continuing debate in microwave chemistry concerns whether microwaves are simply a source of heat (the thermal effect) or whether the microwaves impart some additional effects on the reaction components (the non-thermal effect or sometimes referred to as the specific effect) that also impact on the reaction dynamics [1–3]. In this regard, a study in phase transfer catalysis in solvent-free media, which showed significant differences in reaction dynamics between conventional and microwave heating, led Stuerga and Gaillard [4] to suggest that a very small density of superheated areas (i.e. hot spots) in the system was sufficient to induce a consequent rate enhancement, and that the lack of intrinsic stirring in inorganic solids (e.g. alumina, silica and clays) precludes a uniform distribution of microwave-generated heat by thermal diffusion. Along similar lines, Tsukahara et al. [5] inferred non-equilibrium local heating of dimethylsulfoxide (DMSO) molecules in proximity of Co metallic particles that was induced only by microwave irradiation of the heterogeneous solid–liquid system and not by conventional heating. Such non-equilibrium local heating originates from a faster input of microwave energy relative to slower heat loss induced by thermal gradients between heated micro-domains and surrounding cooler domains.

During the past decade many of our studies in microwave chemistry have attempted to probe the existence of and to delineate the non-thermal effect from the thermal effect in organic syntheses and in TiO_2 photoassisted processes. In the latter case, the photoactivity of various TiO_2 materials from different sources and different compositions in aqueous dispersions improved significantly on simultaneous irradiation with 2.45-GHz microwaves and UV light [2], a phenomenon not encountered by conventional heating at identical temperature. The microwave specific effect was displayed only by the Degussa P-25 TiO_2 specimen [3], which when exposed to 2.45-GHz microwaves the photoactivity was also enhanced in comparison to irradiation with the higher frequency 5.8-GHz microwaves under identical temperature conditions [6].

Earlier we reported the effects of 2.45-GHz microwaves on the Raman lattice phonons of N-doped Degussa P-25 TiO_2 and N-doped

* Corresponding author at: Department of Material & Life Science, Faculty of Science and Technology, Sophia University, 7-1 Kioicho, Chiyodaku, Tokyo 102-8554, Japan.
** Corresponding author. Tel.: +39 0382 98 73 16; fax: +39 0382 98 73 23.
E-mail addresses: horikosi@rs.noda.tus.ac.jp, horikosi@sophia.ac.jp (S. Horikoshi), nick.serpone@unipv.it, nickser@alcor.concordia.ca (N. Serpone).

1010-6030/$ – see front matter © 2011 Elsevier B.V. All rights reserved.
doi:10.1016/j.jphotochem.2011.03.025

Ishihara ST-01 TiO_2 samples [7]. Microwave irradiation of the ST-01 and N-doped N-ST01 TiO_2 samples displayed significant changes in the 144-cm^{-1} optical phonons. Results of the Raman study with the 785-nm laser excitation wavelength inferred a microwave thermal effect on the Ishihara ST-01 and N-ST01 specimens, whereas for the Degussa P-25 samples the microwaves also imparted a specific effect as the microwaves influenced the N-dopant sites in contrast to the ST-01 systems where the dopant sites seemed unaffected as inferred from the temperature–time profiles.

Herein, we examine further the possible existence of a microwave (specific) effect on selected TiO_2 materials (i.e. anatase, rutile, and P-25 TiO_2) using the *in situ* Raman spectroscopic method during irradiation of the samples by 2.45-GHz microwaves (MW) and by simultaneous irradiation with both microwaves and UV radiation (UV/MW) employing a combined microscopic Raman laser (excitation laser line, 532 nm) spectrometer and an assembled microwave applicator. We further probe the photoactivity of all three commercially available materials by re-visiting the degradation dynamics of phenol in aqueous media under UV, UV/MW and UV/CH irradiation conditions. The relation (or lack thereof) between Raman spectral band intensity (lattice optical phonons), photoactivity, and the number of •OH radicals (ESR) produced is examined.

2. Experimental setup

2.1. Microwave- and photo-induced degradation of phenol

The P-25 titanium dioxide specimen was supplied by Degussa, whereas commercial anatase and rutile titanium dioxide specimens were obtained from Wako Pure Chemicals Co. Ltd. (Japan). Some of the characteristic features (e.g. content of anatase, particle sizes, BET specific surface areas, band gaps) of these materials were described previously [3].

An aqueous dispersion of phenol (0.10 mM, 30 mL, initial pH = 5.2) and TiO_2 particles (loading, 60 mg) was placed in a 150-mL Pyrex glass batch-type cylindrical reactor {Taiatsu Techno Co.; size, 160 mm (H) × 37 mm (i.d.)} located in the microwave waveguide (see Figure 1 of Ref. [3]). For these experiments, continuous microwave irradiation was obtained from a Hitachi Kyowa Engineering Co. Ltd. 2.45-GHz microwave generator (maximal power, 800 W) equipped with a power controller, a power monitor, and an isolator (air cooling device). The 60-W continuous microwaves emitted from the magnetron were measured using a power monitor. The reactor was sealed with two Byton O-rings and a stainless steel cap. A pressure gauge and a release bulb were connected to the cover of the reactor.

Unless noted otherwise, temperatures of the phenol/TiO_2 dispersions were measured using an Anritsu Meter Co., Ltd. FL-2000 fiber optic thermometer; dispersion temperature reached 112 °C maximum after 13 min under microwave irradiation, and remained constant thereafter to within the 109–112 °C range. The UV source (Toshiba 75-W Hg lamp; irradiance, ca. 0.5 mW cm^{-2}; maximal emission, 360 nm) was located so as to irradiate the sample reactor through the hole on the side of the microwave waveguide. The dispersion was continually stirred during irradiation. The photodegradation of phenol was probed following three different routes: (a) UV-driven photodegradation (UV); (b) UV-driven and microwave-assisted photodegradation (UV/MW); (c) UV-driven photodegradation with conventional heating (UV/CH) at temperatures otherwise identical to those under UV/MW irradiation. In the UV/CH case, a segment of the cylindrical Pyrex reactor was coated with a metallic film using the metal–organic chemical vapour deposition (MOCVD) technique on one side at the bottom of the reactor to provide the external heat source; applied voltage to the metallic film was <100 V. The uncoated side of the reactor was used to allow the UV light through. The rate of increase of temperature by the UV/MW route was continually monitored during the irradiation period; the applied voltage on the metallic film was then varied to obtain a heating rate for the UV/CH method identical to that of the UV/MW method. That is, the quantity of thermal energy supplied to the photoreactor contents at each irradiation time was the same for both the UV/MW and UV/CH routes. The dynamics of the process were monitored by the loss of UV absorption features of phenol recorded with a JASCO liquid chromatograph (HPLC) equipped with a JASCO UV-2070 UV–vis diode array, a multi-wavelength detector, and a JASCO Crestpak C-18S column. The eluent consisted of a methanol/water solution (1:2, v/v ratio). The relative number of •OH radicals photogenerated in UV- and microwave-irradiated TiO_2 aqueous suspensions was determined relative to a Mn^{2+} standard by DMPO spin-trap ESR spectroscopy (DMPO, 5,5-dimethyl-1-pyrrolidine-*N*-oxide) by a procedure reported earlier [3,8]. Experimental limitations precluded assessing the relative number of •OH radicals produced under the UV/CH conditions (see, e.g. Ref. [8] for a schematic of the equipment).

2.2. In situ observation of Raman spectra

The laser Raman microscopic system was a JASCO Co. system (NRS-5100) integrated into an assembled microwave irradiation applicator (see, e.g. Figure 2 of Ref. [3]). The TiO_2 powdered samples (loading, 0.1 mg) were placed on the microwave irradiation copper dish (ϕ = 8 mm) of the microwave applicator (width, 34 mm; depth, 37 mm; height, 20 mm). Continuous microwave radiation was obtained from a 2.45-GHz microwave semiconductor generator (Fuji Electronic Industrial Co. Ltd.; GNU-201AA; maximal power, 200 W) through a BNC (Bayonet–Neil–Concelman) cable. The applied microwave power was 35.2 W and the reflected microwave power was 0.2 W; the actual microwave applied power was likely less than 30 W owing to possible losses of microwaves in the BNC cable. Microwave radiation incident on the TiO_2 powder on the copper dish was monitored with a 2.45-GHz microwave leak detector (Fuji Electronic Industrial Co. Ltd.). Raman spectra were recorded through a hole (ϕ = 7.8 mm) in the microwave apparatus.

Temperature changes of the TiO_2 powder were monitored with a radiation thermometer. The *in situ* observation of Raman spectra was carried out under microwave irradiation in the dark (MW/dark) and under simultaneous microwave and UV radiations (UV/MW). The incident UV light originated from a fluorescent lamp (irradiance, ca. 0.3 μW cm^{-2} at 360 nm) through the hole on the lid of the microwave applicator. Specimens were UV-irradiated continuously up to 1500 s (i.e. 25 min). The Raman spectra were recorded at 30-s intervals between 0 and 1500 s using the 532-nm laser excitation wavelength. In exploratory experiments we determined an error margin of 2.2% in the peak intensities of the Raman bands for the TiO_2 specimens in the absence of MW and UV irradiation.

3. Results and discussion

3.1. Nature of the P-25 TiO_2

The P-25 TiO_2 consists mostly of well interwoven anatase (ca. 70–80%) and rutile (ca. 20–30%) crystallite forms, depending on the batch, and has been shown to be highly photoactive in photoreductive and photooxidative processes. Details of the microstructure of this photocatalyst are relevant in understanding the photophysical and/or photochemical processes that could limit its efficiency, and that of other titania materials. Bickley et al. [9] suggested that the enhanced photoactivity of P-25 TiO_2 was due to a layer of rutile covering the surface of individual anatase particles that led to a

better separation of photogenerated electrons and holes. By contrast, Datye et al. [10] showed that P-25 consists of single crystallite particles of rutile and anatase phases; no amorphous phase was identified and no particles of anatase covered by a layer of rutile were detected by HRTEM techniques. Ohno et al. [11] re-examined the structural features of P-25 particles by TEM and electron diffraction methods and concluded that their batch of P-25 TiO_2 consisted of 75% anatase and 25% rutile, confirming XRD results reported earlier by others. An intriguing result of their study [11] was that P-25 TiO_2 particles consisted of agglomerates of anatase and rutile elementary particles, with the agglomerates disintegrating under practical operational conditions of photoassisted reactions, with the anatase and rutile particles remaining in close contact. Similarly, Chambers et al. [12] examining the growth of 50-nm thick TiO_2 films on a $LaAlO_3$ substrate at 550 °C at various growth rates showed (bright-field HRTEM images) that rutile particles nucleate within the continuous anatase film surface after the latter started to grow; i.e. a phase-pure epitaxial anatase nucleated at the lower growth rate, whereas at higher growth rates co-nucleation of rutile nanocrystals gave embedded rutile within the continuous anatase film establishing a distinct interface between rutile inclusions and anatase films.

Thus, the intimate mixed phase anatase/rutile microstructure may be the key to the high photoactivity of the P-25 powder resulting from a synergistic effect between the anatase and rutile elementary particles. Hurum et al. [13] probed the charge separation of the mixed-phase P-25 TiO_2 by ESR techniques and deduced that the charges produced on the rutile phase by *visible light* irradiation were stabilized by electron transfer to lower energy lattice trapping sites in the anatase phase. Using Ag^+ ion deposition on the rutile film of a composite film consisting of anatase TiO_2 grown on rutile TiO_2, Kawahara et al. [14] suggested that the high photoactivity of P-25 was due to an increase in charge separation caused by interfacial electron transfer from anatase to rutile. However, this process is muted somewhat when both anatase and rutile are irradiated with UV light commensurate with their band-gaps energies (3.2 eV and 3.0 eV, respectively). The relative photochemical inactivity of pure-phase rutile may be due, in part, to rapid charge carrier recombination [13]. ESR results of Hurum et al. [13] confirmed the assertions of Ohno et al. [11] in that within the mixed-phase P-25 TiO_2 there exists a morphology of nanoclusters that contain atypical rutile crystallites interwoven with the anatase crystallites, with the former acting as a visible-light antenna thereby extending the photoactivity of P-25 to longer wavelengths. The anatase/rutile crystallite structural arrangement in P-25 TiO_2 can potentially create catalytically reactive hot spots at the anatase/rutile interfacial domain [13]. A mixed anatase/rutile specimen with a composition similar to that of P-25 TiO_2 was less photoactive than the latter [3]. The anomaly of the temperature–time profiles of P-25 TiO_2 under microwave irradiation (Fig. 1a) [3] must therefore be due to a better anatase/rutile interfacial construct during the preparation of P-25 TiO_2 at high temperatures by hydrolysis of $TiCl_4$ in a hydrogen flame [10]. Such an interfacial construct should facilitate the charge carrier transfer events.

To gain further insight into the features of P-25 TiO_2 under microwave irradiation, we re-visited the photodegradation of phenol in aqueous P-25 TiO_2 dispersions to assess the effect of microwaves on photoactivity, and to ascertain the involvement of the microwave (specific) effect by comparing the dynamics between the UV/MW and UV/CH irradiation methods used at identical temperatures. We further examined the microwave effect on Raman lattice phonons of P-25 TiO_2 and separately anatase and rutile particles in the solid state as microwave irradiation led to significant differences in the temperature–time profiles (Fig. 1a) and induced a finite increase in *F* centers in P-25 TiO_2

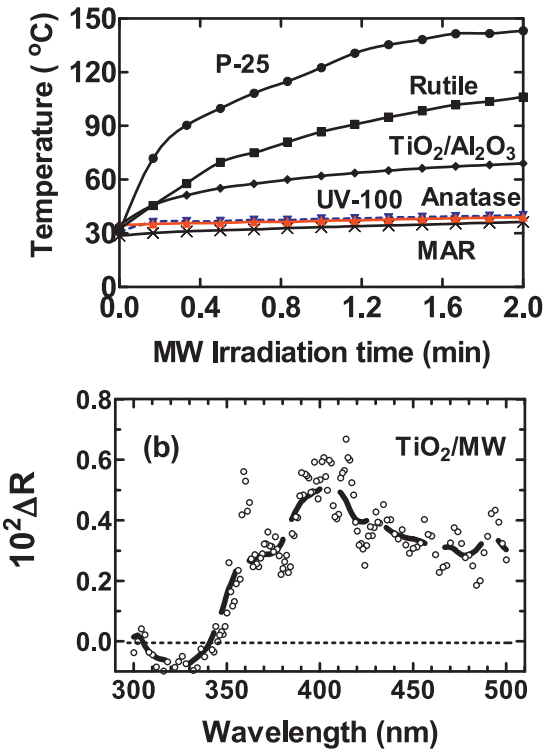

Fig. 1. (a) Temperature-time profiles of the absorption of microwave radiation by powdered TiO_2 specimens packed in a tube. (b) Absorption spectrum as $10^2\,\Delta R$ ($R_{10} - R_0$) of the P-25 TiO_2 after 10 min of microwave irradiation (error ca. ±0.001 in ΔR).
After Horikoshi et al. [3]. Copyright by the American Chemical Society 2009.

after 10 min as evidenced by absorption bands at ~365 nm, 400 nm and at 420–500 nm (Fig. 1b) [3], in line with recent assignments by Kuznetsov and Serpone [15].

3.2. Photoactivity of anatase, rutile, and P-25 TiO_2 specimens used in the Raman study

Control experiments showed that phenol does not degrade under UV irradiation in the absence of TiO_2, and does not degrade under microwave irradiation with or without TiO_2 present. In addition, UV/MW irradiation in the absence of TiO_2 had no consequence on phenol.

For anatase and rutile TiO_2 dispersions, the dynamics of phenol photodegradation showed very little variations (Table 1) irrespective of the methods used to irradiate the metal-oxide samples. By contrast, significant differences occurred in the degradation dynamics involving P-25 TiO_2 dispersions. Comparing the UV and UV/MW methods we note a 2.6-fold faster rate of photodegradation attributable to the microwave thermal factor. Carrying out the photodegradation of phenol by UV irradiation but at a

Table 1
First-order dynamics (k) of the photodegradation of phenol subsequent to 120 min of irradiation of the aqueous TiO_2 dispersions by UV, UV/MW and UV/CH irradiation methods.

TiO_2 sample	k_{deg} (10^{-3} min^{-1})[a]		
	UV	UV/MW	UV/CH
P-25	1.0	2.6	1.6
Anatase	0.6	0.8	0.8
Rutile	0.03	0.04	0.05

[a] Error estimated at ±10%. Note that only the UV/MW and UV/CH data were obtained under identical temperature conditions.

Table 2
Relative number of DMPO–•OH spin-adducts (with respect to a Mn^{2+} standard) produced in aqueous TiO_2 suspensions irradiated with UV light alone (UV), or simultaneously with 2.45-GHz microwaves (3 W) and UV light (UV/MW) for P-25, anatase and rutile TiO_2 specimens.

TiO_2	P-25	Anatase	Rutile
UV	39	22	22
UV/MW	52	18	15

temperature (UV/CH) otherwise identical to that of the UV/MW process, so as to eliminate the thermal factor component, the degradation dynamics are nonetheless ca. 60% faster when microwaves are involved, results somewhat similar to earlier findings on the photoactivity of P-25 TiO_2 toward 4-chlorophenol degradation [3]. Such differences do not preclude a microwave specific (non-thermal) effect; in fact they support the notion of such an effect. Nonetheless, though the data are somewhat limited it is interesting that whenever microwaves are involved together with UV radiation, rates of processes occurring on the surface of P-25 particles are appreciably enhanced.

The number of •OH radicals photogenerated in TiO_2 dispersions is an important factor in the photodegradation dynamics of many organic pollutants [16]. Accordingly, we determined the number of DMPO–•OH spin-adducts by the ESR technique [3,8] produced in the anatase, rutile and P-25 TiO_2 aqueous dispersions when subjected to UV and UV/MW irradiation; results are reported in Table 2. For anatase and rutile dispersions, UV/MW irradiation tended to decrease the number of spin-adducts formed, whereas for P-25 TiO_2 the number of spin-adducts increased 30%. We infer that the microwave energy absorbed by the anatase and rutile TiO_2 samples was converted to thermal energy that affects lattice phonons as evidenced by the Raman data (see below), whereas for P-25 TiO_2 the microwave energy produced additional surface •OH radicals; no Raman spectral intensity changes occurred for the latter sample (Section 3.3).

The greater photoactivity [17–19] (no microwaves) of P-25 TiO_2 in many applications has been attributed consistently to the presence of both anatase and rutile domains within the pristine P-25 nanoparticles [9,11]. Since microwave dielectric heating occurs from the lattice bulk to the surface in contrast to conventional heating [3], which heats the specimen from the surface to the bulk, we hypothesize that microwave irradiation caused additional defect sites to be produced in the lattice and at the surface as evidenced by the result displayed in Fig. 1b. Absorption of microwave energy also causes formation of electron/hole pairs [20]. One factor that determines the ability of TiO_2 to absorb microwave radiation is the presence of free electrons in such an n-type semiconductor. Photogenerated free electrons on the anatase component of P-25 TiO_2 migrate to the rutile domain because of differences in the positions of the lowest energy levels of their respective conduction bands [14]. Accordingly, free and ultimately trapped electrons accumulate in the rutile component of the P-25 particles, so that the local concentration of electrons in the rutile domain will be greater than in either of the separate rutile or anatase TiO_2 particles. This may be one of the reasons for the greater heating efficiency of P-25 under microwave irradiation and for the greater number of •OH radicals produced relative to the anatase and rutile samples reminiscent of the interparticle electron transfer process [21]. Support for such inferences can be found in a recent *in situ* ESR spectroscopic study by Komaguchi et al. [22] who showed that a certain number of excited electrons in the anatase domain migrate through the interfacial boundaries between the anatase/rutile domains to be re-trapped on sites in the rutile domain. Hurum et al. [13] considered such novel interfacial electron trapping sites to be an important and unique feature of the rutile/anatase morphology within P-25 titania, which is critical to the enhanced photoactivity of this mixed-phase TiO_2 photocatalyst.

3.3. In situ Raman spectra

Initial Raman spectra of anatase, rutile and P-25 TiO_2 specimens in the 800–50 cm^{-1} range are illustrated in Fig. 2a–c. Strong to weakly intense lattice vibrational modes (phonons) were seen at 143 cm^{-1} ($E_g^{(1)}$), 397 cm^{-1} (B_{1g}), 515 cm^{-1} ($A_{1g}+B_{1g}$), and 638 cm^{-1} ($E_g^{(2)}$) for anatase TiO_2 (peak intensity ratios were 1.00:0.06:0.05:0.11, respectively); rutile displayed a very weak Raman band at 143 cm^{-1} and more intense bands at 238 cm^{-1}, 446 cm^{-1}, and 610 cm^{-1} (peak intensity ratios were 0.22:0.46:1.00:0.90, respectively), whereas P-25 TiO_2 showed bands at 144 cm^{-1}, 397 cm^{-1}, 516 cm^{-1}, and 639 cm^{-1} (peak ratios, 1.00:0.09:0.09:0.13, respectively). These Raman spectra accord with those previously reported by Balachandran and Eror [23] for pure anatase and rutile polymorphs. Spectra in Fig. 2(d–i) display the time-dependent behavior of the intensity of the most intense Raman bands in each of the TiO_2 samples at 143 cm^{-1}, 446 cm^{-1} and 144 cm^{-1} for anatase, rutile and P-25, respectively, under MW and UV/MW irradiation. The expanded Raman spectra illustrate the absence of spectral shifts and line broadening with irradiation time, but do reveal changes in band intensities.

Fig. 3 illustrates the time changes of the ratios of the most intense Raman spectral bands of each TiO_2 specimen subjected to MW irradiation alone (dark conditions) and UV/MW irradiation relative to the intensities of corresponding bands of initial non-irradiated samples (Fig. 2a–c): for anatase, 143 cm^{-1}; for rutile, 446 cm^{-1}; for P-25, 144 cm^{-1}. X-ray diffraction data, taken using the PANalytical X'Pert pro X-ray diffraction spectrometer, showed that subjecting the anatase, rutile and P-25 TiO_2 specimens to 100-W microwave radiation for 30 min had no effect on the level of anatase versus rutile in the samples, clearly indicating that no phase changes occurred during the microwave treatment of the solid specimens.

Microwave irradiation of TiO_2 powdered samples for 300 s showed a slight increase of temperature: 4 °C for anatase, 7 °C for rutile, and 6 °C for P-25. Such smaller than expected temperature increases from the conversion of microwave energy were unlikely to affect the Raman band intensities as temperature-dependent Raman spectral shifts and band intensity changes in bulk and dispersed metal oxides occurs over several hundred degrees [24]. Note that the 2.45-GHz microwave energy (1×10^{-5} eV) is some five orders of magnitude lower than the band gap energy of TiO_2 (3.0–3.2 eV). In addition, such changes in intensity as seen here cannot be attributed to changes in particle size since, as Kelly et al. have noted [25], a decrease in particle size of TiO_2 would cause the Raman signal to broaden asymmetrically, to shift to the blue, and to decrease in intensity, features particularly pronounced for the 142 cm^{-1} Raman peak of their TiO_2 samples. In our case, it is relevant to reiterate that neither spectral shifts nor line broadening (asymmetrically or otherwise) were observed for all three TiO_2 samples examined (Fig. 2).

The intensity of a Raman spectral band is proportional to the molecular density N and the polarizability α, as expressed by Eq. (1) [26]:

$$\text{Intensity} \approx N\alpha^2 \approx N\left(\left(\frac{\delta\alpha}{\delta Q}\right)_0 Q\right)^2 \quad (1)$$

where Q denotes the normal coordinates. Considering that the molecular density of the TiO_2 samples suffers no changes when the specimens are subjected to microwave radiation (XRD results), the variations in peak intensities must then be due to polarizability changes in the TiO_2 crystalline particles. Decreases of Raman

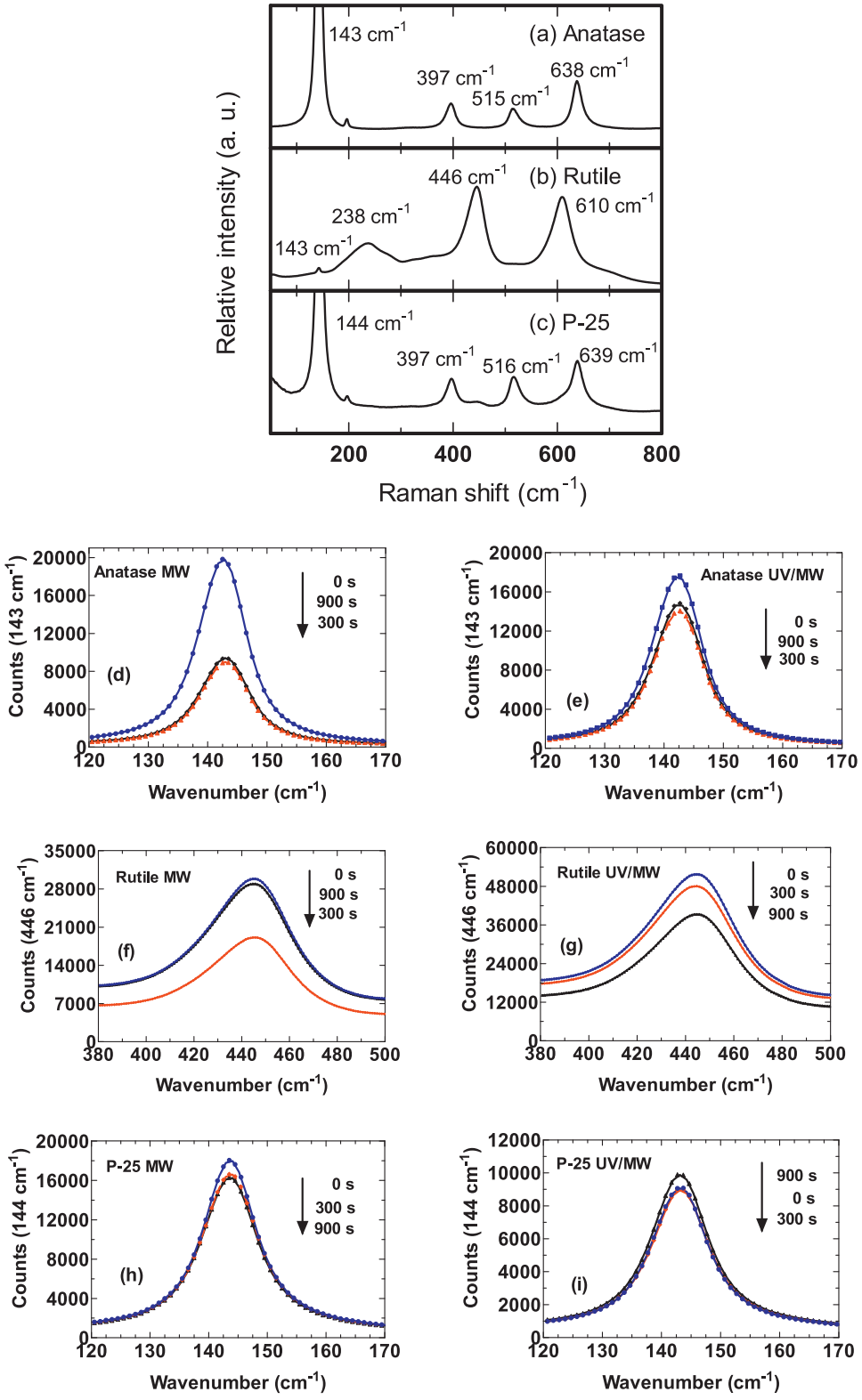

Fig. 2. (a–c) Raman spectra of anatase, rutile and P-25 TiO_2 specimens prior to being subjected to either MW irradiation alone or to UV/MW irradiation. Other spectra illustrate the time-dependent behavior (or lack thereof) of the most intense Raman-active bands under MW irradiation alone for (d) anatase at 143 cm^{-1}, (f) rutile at 446 cm^{-1}, and (h) P-25 titania at 144 cm^{-1}; under simultaneous irradiation by both UV and MW radiations for (e) anatase at 143 cm^{-1}, (g) rutile at 446 cm^{-1}, and (i) P-25 at 144 cm^{-1}. Note the absence of band shifts and line broadening with irradiation time.

band intensities could (in principle) be caused by irregular lattice vibrations owing to differences in bond lengths in the different TiO_2 crystals subsequent to the influence of the microwaves' electric field, which induces a dipole moment (μ_{ind}) on the ensemble of Ti–O bonds with the polarizability α decreasing with increasing electric field; that is $\alpha = \mu_{ind}/E$. For constant electric field E, the polarizability varies with the overall average induced bond dipole moments. The electronic polarizabilities of Ti^{4+} and O^{2-} ions are

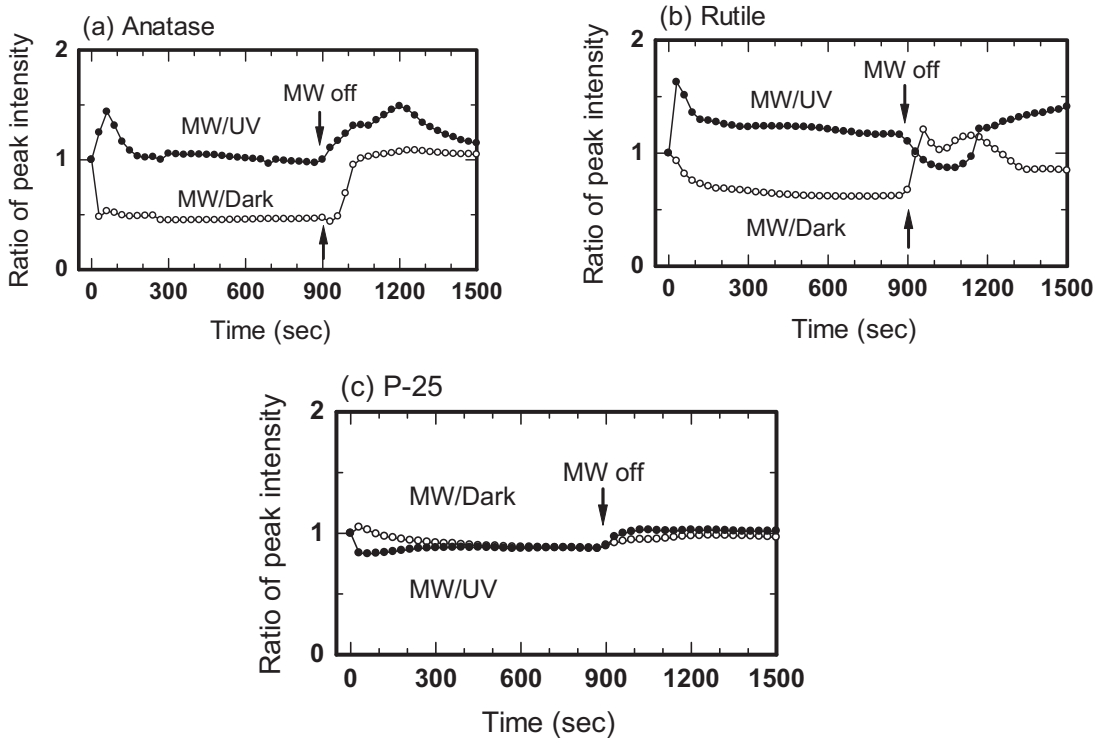

Fig. 3. Time-dependent changes of the peak intensity ratios of the Raman spectral bands of anatase, rutile and Degussa P-25 TiO_2 powdered specimens under microwave irradiation alone (MW) and under simultaneous combined UV and MW irradiation. Ratios were calculated automatically with baseline correction and relative to the bands of the non-irradiated samples taken as time 0 for anatase (143 cm^{-1}), for rutile (446 cm^{-1}), and for the P-25 TiO_2 sample (144 cm^{-1}).

0.19 and 2.2 A^3, respectively [27], so that the microwaves' electric field is expected to have a greater influence on the O^{2-} ions in the bulk lattice and on the particle surface. To ascertain that our observations were not an artifact of the experimental setup and technique used, we recorded the Raman spectrum of a quartz crystal (SiO_2), a well known non-absorber of microwave radiation, under otherwise identical conditions to those used for the TiO_2 systems. We observed neither a change in peak intensity nor a shift of the Raman spectral bands, so that an artifact is precluded. Thus, changes in band intensities are due to interactions of the microwaves with anatase and rutile TiO_2.

3.3.1. Anatase and rutile samples

Peak intensities of the 143 cm^{-1} and 446 cm^{-1} Raman bands in anatase and rutile, respectively, showed a remarkable decrease under microwave irradiation alone and remained fairly constant until the MW radiation was turned off (900 s), at which time the ratio tended toward the initial value of 1.0. By comparison, the intensity ratio of the P-25 specimen displayed a negligible downward trend with time under MW irradiation alone, returning to the initial ratio of 1.0 on termination of the microwaves.

Peak intensity ratios for anatase and rutile samples increased immediately upon simultaneous UV/MW irradiation of these specimens (1.4 at 60 s and 1.6 at 30 s, respectively). The ratios subsequently decreased to reach a constant value. When the microwave radiation was turned off at 900 s (Fig. 3a), the peak intensity ratio (1.5 at 1200 s) for anatase returned to the value observed at the 30-s time period, whereas the ratio for rutile decreased further (Fig. 3b).

Germane to the above discussion on the anatase and rutile samples, Xie et al. [24] showed that the intensities of Raman spectral bands of bulk and dispersed metal oxides (e.g. Nb_2O_5, MoO_3, WO_3, and V_2O_5) are temperature-dependent when significant optical absorption occurs in the frequency range corresponding to the excitation Raman line. Such temperature effects are typically seen as losses in spectral intensities and as spectral shifts to higher energy. Changes in band intensities and Raman shifts appear to be particularly critical for bulk and dispersed metal oxides that exhibit a band edge in the vicinity of the laser excitation wavelength since an increase in optical absorption of the oxide could lead to a decrease in the sampling depth for Raman and thus to a loss in spectral intensity [24]. Metal oxides with absorption band edges far from the wavelength of the laser line, however, are not expected to be affected by temperature. In the present cases, the absorption edges of the anatase and P-25, and of rutile at 387 nm and 400 nm, respectively, were significantly different from the laser excitation wavelength (532 nm), thus precluding optical absorption by the TiO_2 specimens. None of the three TiO_2 samples examined herein showed spectral shifts (see Fig. 2).

Scheme 1 illustrates our view, albeit a simplistic one, of the proposed effects of microwave and microwave/ultraviolet irradiations on the anatase and rutile polymorphs. Under MW/dark conditions, we deduce that the Raman intensities decrease owing to formation of oxygen vacancies (V_O) induced by the microwave radiation fields as attested for the P-25 TiO_2 sample in Fig. 1b yielding *F*-type color centers [15,30]. By contrast, under MW/UV irradiation the Raman intensities promptly increase at first, owing to the UV photogenerated mobile charge carriers in the conduction band (electrons) that lead to an overall increase in polarizability, subsequent to which the intensity ratios decrease back to ca. 1 for anatase and close to 1 for rutile owing to opposing effects between generation of photoelectrons by UV and formation of oxygen vacancies (or other defects) by the microwave radiation fields that trap the electrons to form color centers such as *F*-centers and Ti^{3+} centers [15,30]. Termination of the microwave radiation at 900 s causes intensity ratios to return to 1 except under continued UV irradiation which causes the number of photogenerated electrons to increase at first followed by a decrease of the ratios as the electrons get trapped in electron traps or otherwise are trapped by the ubiquitously present chemisorbed oxygen at the particle surface.

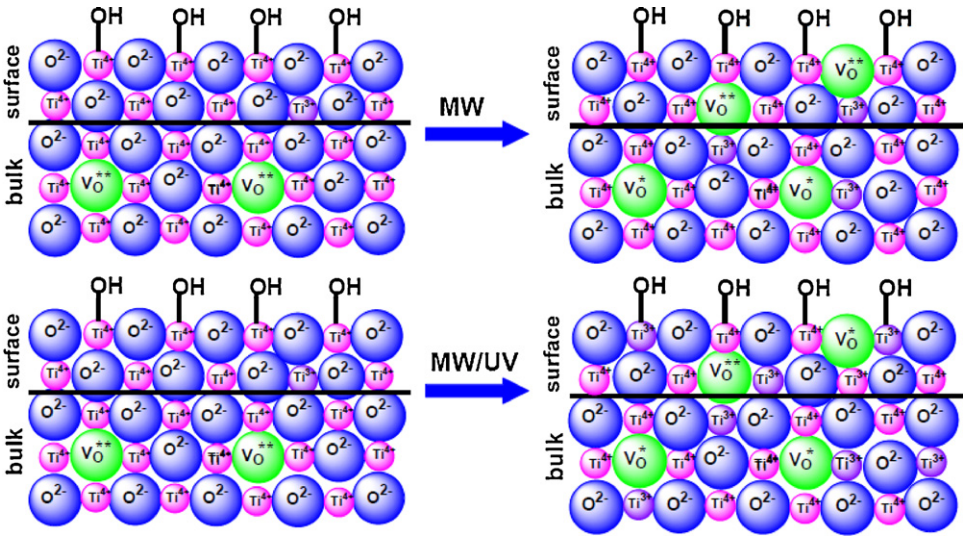

Scheme 1. Simplified view of the effects of microwave and microwave/ultraviolet irradiation on the anatase and rutile polymorphs that lead to formation of *F* and Ti^{3+} color centers.

3.3.2. *P-25 titanium dioxide*

Unlike the anatase and rutile polymorphs, only negligible changes occurred in the Raman spectral intensities of P-25 TiO_2 (Fig. 3c) under both MW and MW/UV irradiations. That is, the Raman spectral intensities are severely curtailed by the microwave effect with or without concomitant UV radiation. This is likely the result of the nature of the P-25 TiO_2 hetero-architecture of a rutile domain (or particle) strongly coupled (fused) to anatase [12] that resulted from the manner by which P-25 is produced in the high temperature H_2 flame in the presence of oxygen (precursor, $TiCl_4$). The interfacial construct between the rutile and the anatase is perhaps the major defect in P-25 TiO_2 which, under applied microwave radiation fields, likely causes the accumulation of photogenerated charge carriers at this interface (interfacial or space-charge polarization [28]).

Also germane to the present discussion, Deskins et al. [29] performed molecular dynamics simulation of interfaces between rutile and anatase surfaces of TiO_2 in attempts to understand the interfaces produced in mixed-phase photocatalysts, such as P-25 TiO_2, and as a first step toward characterizing electron–hole transport in such photoactive materials. The rutile (1 1 0) and anatase (1 0 1) surfaces are the most abundant surfaces on titania crystals, and to the extent that these surfaces are the most stable and have the largest commensurate structures, it was not surprising that the rutile (1 1 0) surface should bind most strongly to the (1 0 1) anatase surface and form preferentially $(1\,1\,0)_R$–$(1\,0\,1)_A$ interfaces [29]. The simulations also revealed little distinction between rutile and anatase surfaces at the interface, with both phases experiencing an increase in coordination of the five-coordinate Ti atoms to six-coordinate Ti relative to the free surfaces. Two additional and most significant observations emerged from the study of Deskins et al. [29]: the interfaces are slightly disordered, with the disorder limited to a narrow region at the interface down to a depth of ca. 4 Å; formation of rutile octahedral structures appears to occur on the anatase side of the interface as a result of surface rearrangement.

In spite of the above simulations, however, we do not preclude the possibility that, in the actual preparation of P-25 TiO_2 batches, oxygen vacancies are produced at the anatase–rutile interfaces whenever slightly oxygen-deficient growth conditions prevail during the manufacturing process [12], and/or that during the formation of the interfaces these oxygen vacancies form during the interfacial construct with or without oxygen deficiencies.

4. Concluding remarks

In summary, we deduce from the presently available data and the above discussion that the microwave energy absorbed by the P-25 TiO_2 system was consumed to bring about changes at the interfacial boundaries between the coupled rutile and anatase polymorphic structures. Further, such changes may lead to generation of oxygen vacancies, well known to trap conduction band electrons to yield *F*-type color centers [13,30], thereby allowing the valence band holes to produce additional •OH radicals as evidenced by the ESR results of Table 2, unlike the anatase and rutile samples where the number of •OH radicals decreased on UV/MW combined irradiation relative to UV irradiation alone. The resulting increased charge separation within the P-25 particles and the greater number of •OH radicals are consistent with the increased rate enhancements and greater photoactivity witnessed in the results of Table 1, not otherwise seen for the anatase and rutile samples. Rather, in the latter two cases the microwave energy absorbed by the anatase and rutile specimens was probably consumed by bringing about (mostly) changes to the polarizability of the Ti–O bonds through interactions with the microwave electric field, thereby affecting the band intensities of Raman-active lattice phonons as witnessed experimentally (Figs. 2 and 3). While it is tempting to generalize our observations and inferences to other TiO_2 samples, we cannot preclude the notion that just as the photoactivity of TiO_2 systems from different sources depends on how they were produced and on how they may have been pre-treated, so could the microwave effects differ on other TiO_2 specimens. Nonetheless, a specific microwave effect seems indicated by the available data reported thus far.

Acknowledgments

Financial support to S.H. from the Japan Society for the Promotion of Science (JSPS) through a Grant-in-aid for young scientists is gratefully appreciated. One of us (N.S.) thanks Prof. Albini of the University of Pavia for the constant gracious hospitality during the winter semesters in his laboratory (since 2002). We are also grateful to Dr. Ohokubo of the JASCO Co. for technical assistance with the Raman spectroscopy and for the microwave generator, and also to Mr. Yoshida of Fuji Electronic Industrial Co. Ltd. for assistance.

References

[1] N. Serpone, S. Horikoshi, A.V. Emeline, Microwaves in advanced oxidation processes for environmental applications. A brief review, J. Photochem. Photobiol. C: Photochem. Rev. 11 (2010) 114–130.

[2] S. Horikoshi, N. Serpone, Photochemistry with microwaves: catalysts and environmental applications, J. Photochem. Photobiol. C: Photochem. Rev. 10 (2009) 96–110.

[3] S. Horikoshi, F. Sakai, M. Kajitani, M. Abe, A.V. Emeline, N. Serpone, Microwave-specific effects in various TiO_2 specimens. Dielectric properties and degradation of 4-chlorophenol, J. Phys. Chem. C 113 (2009) 5649–5657.

[4] D. Stuerga, P. Gaillard, Microwave heating as a new way to induce localized enhancements of reaction rate. Non-isothermal and heterogeneous kinetics, Tetrahedron 52 (1996) 5505–5510.

[5] Y. Tsukahara, A. Higashi, T. Yamauchi, T. Nakamura, M. Yasuda, A. Baba, Y. Wada, *In situ* observation of non-equilibrium local heating as an origin of special effect of microwave on chemistry, J. Phys. Chem. C 114 (2010) 8965–8970.

[6] S. Horikoshi, F. Sakai, M. Kajitani, M. Abe, N. Serpone, Microwave frequency effects on the photoactivity of TiO_2: dielectric properties and the degradation of 4-chlorophenol, bisphenol A and methylene blue, Chem. Phys. Lett. 470 (2009) 304–307.

[7] S. Horikoshi, Y. Minatodani, H. Sakai, M. Abe, N. Serpone, Characteristics of microwaves on second generation nitrogen-doped TiO_2 nanoparticles and their effect on photoassisted processes, J. Photochem. Photobiol. A: Chem. 217 (2011) 191–200.

[8] S. Horikoshi, H. Hidaka, N. Serpone, Hydroxyl radicals in microwave photocatalysis. Enhanced formation of $^{\bullet}OH$ radicals probed by ESR techniques in microwave-assisted photocatalysis in aqueous TiO_2 dispersions, Chem. Phys. Lett. 376 (2003) 475–480.

[9] R.I. Bickley, T. Gonzalez-Carreno, J.S. Lees, L. Palmisano, R.J.D. Tilley, A structural investigation of titanium dioxide photocatalysts, J. Solid State Chem. 92 (1991) 178–190.

[10] A.K. Datye, G. Riegel, J.R. Bolton, M. Huang, M.R. Prairie, Microstructural characterization of a fumed titanium dioxide photocatalyst, J. Solid State Chem. 115 (1995) 236–239.

[11] (a) T. Ohno, K. Sarukawa, K. Tokieda, M. Matsumura, Morphology of a TiO_2 photocatalyst (Degussa, P-25) consisting of anatase and rutile crystalline phases, J. Catal. 203 (2001) 82–86;
(b) T. Ohno, K. Sarukawa, M. Matsumura, Photocatalytic activities of pure rutile particles isolated from TiO_2 powder by dissolving the anatase component in HF solution, J. Phys. Chem. B 105 (2001) 2417–2420.

[12] S.A. Chambers, C.M. Wang, S. Thevuthasan, T. Droubay, D.E. McCready, A.S. Lea, V. Shutthanandan, C.F. Windisch, Epitaxial growth and properties of MBE-grown ferromagnetic Co-doped TiO_2 anatase films on $SrTiO_3(0\,0\,1)$ and $LaAlO_3(0\,0\,1)$, Thin Solid Films 418 (2002) 197–210.

[13] D.C. Hurum, K.A. Gray, T. Rajh, M.C. Thurnauer, Recombination pathways in the Degussa P25 formulation of TiO_2: surface versus lattice mechanisms, J. Phys. Chem. B 109 (2005) 977–980.

[14] T. Kawahara, Y. Konishi, H. Tada, N. Tohge, J. Nishii, S. Ito, A patterned TiO_2(anatase)/TiO_2(rutile) bilayer-type photocatalyst: effect of the anatase/rutile junction on the photocatalytic activity, Angew. Chem., Int. Ed. 41 (2002) 2811–2813.

[15] V.N. Kuznetsov, N. Serpone, On the origin of the spectral bands in the visible absorption spectra of visible-light-active TiO_2 specimens: analysis and assignments, J. Phys. Chem. C 113 (2009) 15110–15123.

[16] R.W. Matthews, Hydroxylation reactions induced by near-ultraviolet photolysis of aqueous titanium dioxide suspensions, J. Chem. Soc., Faraday Trans. I 80 (1984) 457–471.

[17] The photoactivity of various TiO_2 specimens in photoassisted processes is best described by determining the quantum yield of the processes for different batches of TiO_2 samples as proposed earlier by Serpone and Salinaro [18] and Salinaro et al. [19] when only UV radiation activated the metal oxide particles. In the present instance, however, there are no protocols to assess the quantum yields of processes that also involve microwave radiation on the one hand and conventional heating on the other. Nonetheless, under constant experimental conditions of UV and microwave irradiation the photoactivity of the various TiO_2 samples can be assessed on the basis of the dynamics of the processes.

[18] N. Serpone, A. Salinaro, Terminology, relative photonic efficiency, and quantum yields in heterogeneous photocatalysis. Part I. Suggested protocol, Pure Appl. Chem. 71 (1999) 303–320.

[19] A. Salinaro, A. Emeline, J. Zhao, H. Hidaka, V. Ryabchuck, N. Serpone, Terminology, relative photonic efficiency, and quantum yields in heterogeneous (solid/liquid) photo-catalysis. Part II. Experimental determination of quantum yields, Pure Appl. Chem. 71 (1999) 321–335.

[20] J.M. Warman, M.P. de Haas, P. Pichat, N. Serpone, Effect of isopropyl alcohol on the surface localization and recombination of conduction-band electrons in Degussa P-25 TiO_2. A pulse-radiolysis time-resolved microwave conductivity study, J. Phys. Chem. 95 (1991) 8858–8861.

[21] N. Serpone, E. Borgarello, M. Graetzel, Visible light induced generation of hydrogen from CdS in mixed semiconductor dispersions; improved efficiency through inter-particle electron transfer, J. Chem. Soc., Chem. Commun. (1984) 342–344.

[22] K. Komaguchi, H. Nakano, A. Araki, Y. Harima, Photoinduced electron transfer from anatase to rutile in partially reduced TiO_2 (P-25) nanoparticles: an ESR study, Chem. Phys. Lett. 428 (2006) 338–342.

[23] U. Balachandran, N.G. Eror, Raman spectra of titanium dioxide, J. Solid State Chem. 42 (1982) 276–282.

[24] S. Xie, E. Iglesia, A.T. Bell, Effects of temperature on the Raman spectra and dispersed oxides, J. Phys. Chem. B 105 (2001) 5144–5152.

[25] S. Kelly, F.H. Pollak, M. Tomkiewicz, Raman spectroscopy as a morphological probe for TiO_2 aerogels, J. Phys. Chem. B 101 (1997) 2730–2734.

[26] T. Kitagawa, A.T. Tu, Introduction to Raman Spectroscopy, Kagaku-Dojin Publishing Co., Inc., Kyoto, Japan, 1988, ISBN:4-7598-0172-3 (in Japanese).

[27] J.R. Tessman, A.H. Kahn, W. Shockley, Electronic polarizabilities of ions in crystals, Phys. Rev. 92 (1953) 890–895.

[28] S.K. Arora, V. Patel, B. Amin, A. Kothari, Dielectric behaviour of strontium tartrate single crystals, Bull. Mater. Sci. 27 (2004) 141–147.

[29] N.A. Deskins, S. Kerisit, K.M. Rosso, M. Dupuis, Molecular dynamics characterization of rutile–anatase interfaces, J. Phys. Chem. C 117 (2007) 9290–9298.

[30] A.V. Emeline, V.N. Kuznetsov, V.K. Ryabchuk, N. Serpone, Visible-light-active titania photocatalysts: the case of N-doped TiO_2s—properties and some fundamental issues, Int. J. Photoenergy (2008), doi:10.1155/2008/258394.